We are IntechOpen, the world's leading publisher of Open Access books Built by scientists, for scientists

4,800
Open access books available

122,000
International authors and editors

135M
Downloads

Our authors are among the

154
Countries delivered to

TOP 1%
most cited scientists

12.2%
Contributors from top 500 universities

CLARIVATE ANALYTICS BOOK CITATION INDEX INDEXED

WEB OF SCIENCE™

Selection of our books indexed in the Book Citation Index in Web of Science™ Core Collection (BKCI)

Interested in publishing with us?
Contact book.department@intechopen.com

Numbers displayed above are based on latest data collected.
For more information visit www.intechopen.com

Chapter 3

Application of Fuzzy Logic Control for Grid-Connected Wind Energy Conversion System

Jianzhong Zhang and Shuai Xu

Additional information is available at the end of the chapter

http://dx.doi.org/10.5772/59923

1. Introduction

Recent years have seen rapid development in wind energy across the world due to rising pollution levels and worrying changes in the global climate [1]. China is the world's largest investor in wind energy and has set ambitious targets for renewable energy. At the end of 2012, the installed capacity of wind farms in the world had reached 282.5 GW, an increase of 19% compared with 2011. Wind power may become China's third most important power resource by 2020, with an expected installed capacity of 200 GW [2].

In the variable-speed wind-energy conversion system (WECS), wind turbines can operate as close as possible to optimal speed to realize maximum power point tracking (MPPT) for various wind-speeds [3-6]. To take advantage of the higher energy capture and increased system compliance available from variable speed operation, power electronics interfaces must be provided between the machine terminals and the grid. The back-to-back pulse width modulation (PWM) converter-based power electronic interface is a suitable option for the generator in wind-power applications, where the permanent magnet (PM) generator can offer high efficiency and high power density. These advantages make it very attractive for variable speed WECS, as shown in Figure 1 [7-10].

Two power electronic converters have to be co-operatively controlled to keep a constant direct current-link (DC-link) voltage. The voltage source of the DC link enables both PWM converters to operate at high efficiency. The generator-side converter keeps the wind turbine-generator system operating at an overall optimal level by controlling the generator torque and adjusting the reactive power exchanged between the rectifier and the generator. The grid-side converter plays an important role in the control of power transformation and power quality [7].

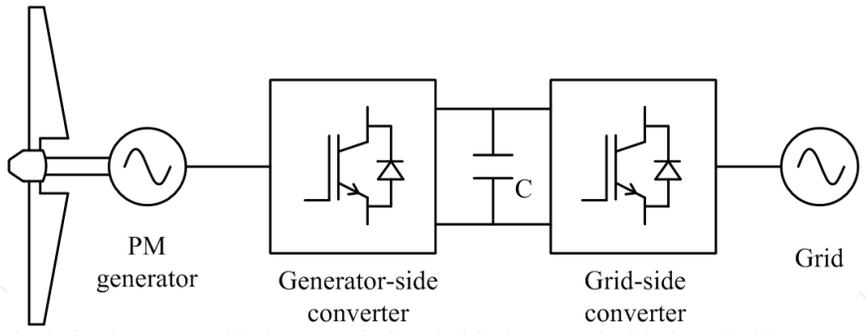

Figure 1. Variable-speed wind-energy conversion system

This book chapter presents the significance and effectiveness of the fuzzy-logic-based control strategies for grid-connected WECS in solving the fluctuation of DC-link voltage. The chapter is organized as follows. Firstly, the model of the grid-connected PWM converter is presented, and the DC-link voltage fluctuation is analysed. Secondly, three fuzzy-logic-control (FLC)-based control strategies are proposed for the DC-link voltage control. Finally, a simulation model of WECS is constructed by using the MATLAB/Simulink tool, where the steady- and transient-state performances of the proposed fuzzy-logic-based controllers are simulated and compared.

2. Model of grid-connected PWM converter

The simplified three-phase PWM converter is shown in Figure 2. Because the inductance parameters have better ability in current harmonic suppression than the L filter in the same case, the LCL filter is adopted in the WECS [5].

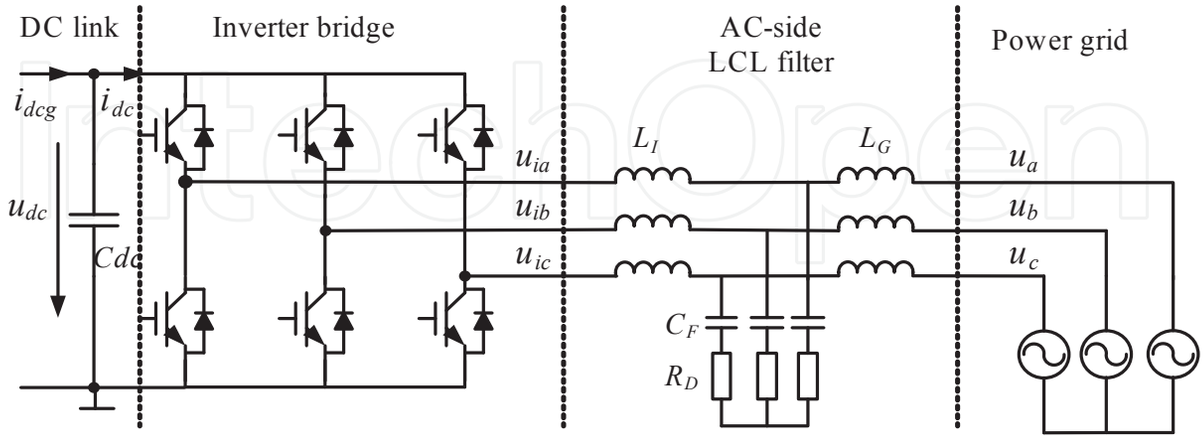

Figure 2. The simplified three-phase PWM converter

The three-phase symmetrical system can be expressed by the single-phase equivalent circuit, as shown in Figure 3.

http://dx.doi.org/10.5772/59923

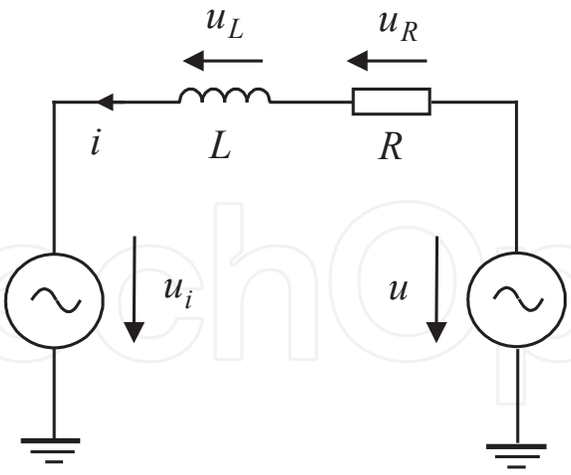

Figure 3. Single-phase equivalent circuit of PWM converter

The voltage balance equation, according to the single-phase equivalent circuit shown in Figure 3, can be written as follows:

$$\begin{bmatrix} u_a \\ u_b \\ u_c \end{bmatrix} = L\frac{d}{dt}\begin{bmatrix} i_a \\ i_b \\ i_c \end{bmatrix} + R\cdot\begin{bmatrix} i_a \\ i_b \\ i_c \end{bmatrix} + \begin{bmatrix} u_{ia} \\ u_{ib} \\ u_{ic} \end{bmatrix} \tag{1}$$

Under the synchronous rotating coordinate system, ignoring the resistance voltage drop and assuming that $d_{\omega g}/dt$=const, we can obtain the following model:

$$\begin{bmatrix} u_d \\ u_q \end{bmatrix} = L\frac{d}{dt}\begin{bmatrix} i_d \\ i_q \end{bmatrix} + \begin{bmatrix} R & -\omega_g L \\ \omega_g L & R \end{bmatrix}\cdot\begin{bmatrix} i_d \\ i_q \end{bmatrix} + \begin{bmatrix} u_{id} \\ u_{iq} \end{bmatrix} \tag{2}$$

The converter system can be expressed as an ideal switch model, and the AC-side phase to ground voltage of converter is given as

$$\begin{cases} u_{ia} = \dfrac{u_{dc}}{3}(2S_A - S_B - S_C) \\ u_{ib} = \dfrac{u_{dc}}{3}(-S_A + 2S_B - S_C) \\ u_{ic} = \dfrac{u_{dc}}{3}(-S_A - S_B + 2S_C) \end{cases} \tag{3}$$

where $S_k = 1$ (the upper bridge turns on, the lower bridge turns off); $S_k = 0$ (the upper bridge turns on, the lower bridge turns off), $k = A, B, C$. The DC-link voltage and the current of converter is expressed as

$$\begin{cases} C_{dc}\dfrac{du_{dc}}{dt} = i_{dcg} - i_{dc} \\ i_{dc} = S_A i_a + S_B i_b + S_C i_c \end{cases} \tag{4}$$

3. Wind-energy extraction and DC-link voltage fluctuations

The mechanical power of the wind turbine extracted from the wind is

$$P_w = 0.5 C_p(\beta, \lambda)\rho A \upsilon^3 \tag{5}$$

where ρ is density of air, A is area swept by blades, υ is wind-speed, C_p is the power coefficient of the wind turbine, β is the blade pitch angle and λ is the tip speed ratio.

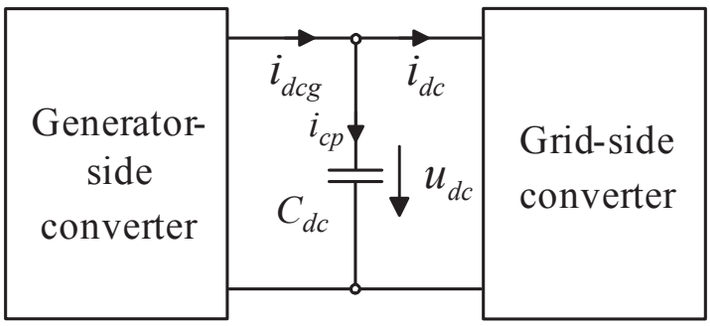

Figure 4. Diagram of DC-link capacitor

The back-to-back PWM converter is composed of a grid-side converter, a generator-side converter and a DC-link capacitor. The mechanical power is transferred into electrical power by the PM generator and output to the generator-side converter. From the diagram of the DC-link capacitor shown in Figure 4, the relationship between the DC-link voltage of the capacitor and the current can be obtained as

$$i_{cp} = C_{dc}\frac{du_{dc}}{dt} = i_{dcg} - i_{dc} \tag{6}$$

where C_{dc} is the capacitance of the DC-link capacitor, u_{dc} is the DC-link voltage of the capacitor, i_{dcg} is the current of the generator-side converter output to the DC link, and i_{dc} is the current output to the grid.

At low wind-speed below the rated condition, the PM generator is supposed to work in MPPT strategy. Then, for a well-designed generator-side control system, a simple model for the generator-side converter may be used where the electrical power injected to the DC link is proportional to the cube of the wind-speed, as follows:

http://dx.doi.org/10.5772/59923

$$P_{rc} = u_{dc} i_{dcg} = k\upsilon^3 \tag{7}$$

where k is the factor related to the wind turbine system. The injection current i_{dcg} can be expressed as

$$i_{dcg} = \frac{k\upsilon^3}{u_{dc}} \tag{8}$$

where the current i_{dcg} inputs to the DC link and affects the DC-link voltage variations.

In the back-to-back PWM converter of the WECS, the power is transferred between the generator-side and the grid-side converter. Ignoring the power losses of the power electronic devices and supposing the DC-link voltage constant, the input power from the generator-side converter should be equal to the output power of the grid-side converter:

$$P_{rc} = P_{gc} \tag{9}$$

where P_{gc}, P_{rc} are the instantaneous power of the grid-side converter and generator-side converter.

Due to the stochastic wind-speed in the natural condition, the power absorbed by the wind turbine is dynamically varied and transferred from the generator-side converter to the grid-side converter. Then, the DC-link capacitor is used as energy buffer and the instantaneous power of the DC-link capacitor is given as

$$P_c = u_{dc} i_{cp} = C u_{dc} \frac{du_{dc}}{dt} \tag{10}$$

where i_{cp} is the current of the DC-link capacitor. The variation of the instantaneous power will generate the current of the DC-link capacitor, according to equation (10). As a consequence, the DC-link voltage is fluctuated, where the voltage fluctuation is proportional to the imbalanced power flow between the generator-side converter and grid-side converter during the dynamic regulation of the WECS. Here, the current balance equation is as follows:

$$i_{dc} = i_{dcg} - i_{cp} = \frac{kv^3}{u_{dc}} - C_{dc} \frac{du_{dc}}{dt} \tag{11}$$

By combining (4) and (11), the relationship between the AC-side current and DC-link voltage of converter can be expressed as

$$i_a S_A + i_b S_B + i_c S_C = \frac{kv^3}{u_{dc}} - C \frac{du_{dc}}{dt} \tag{12}$$

It can be seen in (12) that the DC-link voltage ripples will inevitably influence the waveforms of the grid-side current. In the actual operation of the WECS, the turbulence of the wind will generate dynamic power variations and increase the DC-link voltage ripples. This will result in deterioration of power quality on the grid side, and the DC-link voltage control strategy thus becomes an important issue for the WECS. Recently, several DC-link voltage control strategies have been proposed and applied in the WECS [11-13]. In the following parts, fuzzy-logic-based as well as traditional PI-based DC-link voltage control strategies are described and simulated in the MATLAB/Simulink environment. Simulation results are discussed and compared to verify the effectiveness of the proposed control strategies.

4. Traditional PI-based control strategy

The mathematical model of continuous-time linear PID controller in position form is described as

$$u(t) = K(e(t) + \frac{1}{T_i}\int_0^t e(\tau)d\tau + T_d\frac{de(t)}{dt}) \tag{13}$$

where $e(t)$ is the error input signal, K is a gain, T_i is integral time, and T_d is derivative time. In some application fields, full PID control is sometimes not desired, to some extent. This is because the derivative term tends to amplify noise, which should be avoided when applied for the voltage source inverter (VSI). When T_d is set to zero, the PID controller becomes a PI controller. Hence, the incremental form of the PI controller is described as

$$u(t) = K(e(t) + \frac{1}{T_i}\int_0^t e(\tau)d\tau) \tag{14}$$

The corresponding discrete-time position form is described as

$$u(n) = K(e(n) + \frac{T}{T_i}\sum_{i=0}^{n} e(i)) = K_p e(n) + K_i\sum_{i=0}^{n} e(i) \tag{15}$$

where T is the sampling period. K_p, K_i are the proportional gain and integral gain of the PI controller, respectively.

The PI controller is often used in the incremental form, which calculates change of the controller output. Note that at time n-1,

$$u(n-1) = K(e(n-1) + \frac{T}{T_i}\sum_{i=0}^{n-1} e(i)) = K_p e(n-1) + K_i\sum_{i=0}^{n-1} e(i) \tag{16}$$

The PI controller has the advantages of simple structure, good stability, and high reliability, and is especially suitable for the established accurate mathematical model of the control

http://dx.doi.org/10.5772/59923

system. The PI controller has been widely applied to the control system of the WECS. The control block diagram of a traditional PI-based vector control strategy for the grid-side converter is shown in Figure 5. The grid-side converter is controlled with a vector decoupling control strategy and the grid voltage orientation. The active power and reactive power can be independently controlled with the double closed-loop strategy, where the outer loop is the DC-link voltage controller and the inner loop is the current controller [13].

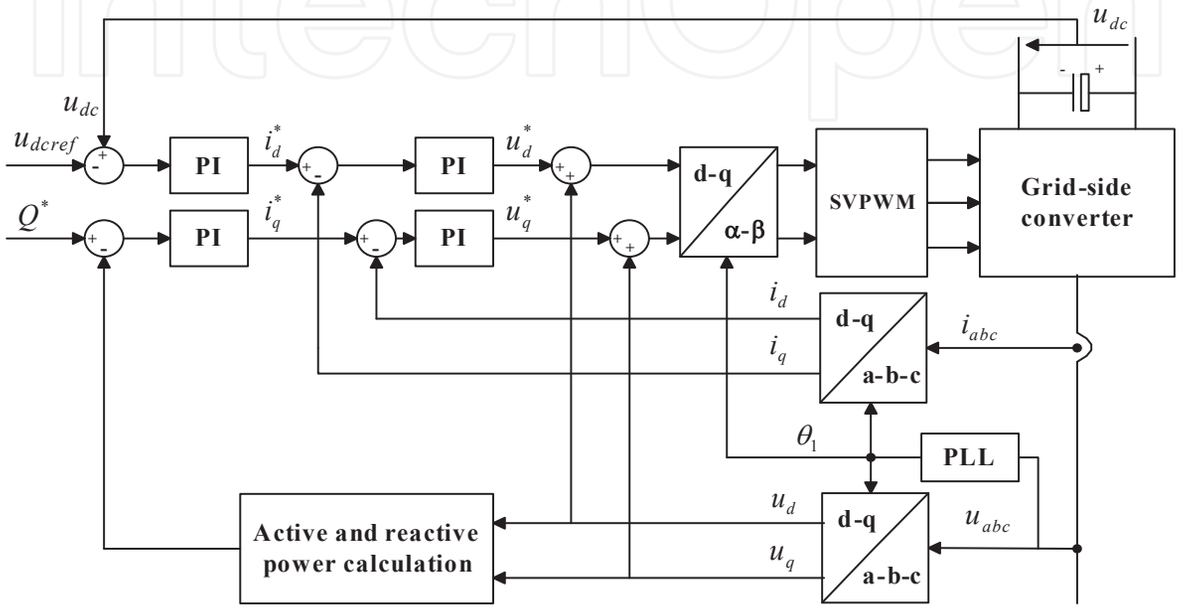

Figure 5. Traditional PI-based vector control strategy

5. Fuzzy logic control strategies of grid-connected converter

Since the PI control depends on the precise mathematical model, the PI control performance becomes poor when there is disturbance of the system parameters or stochastic variations of wind-speed. Moreover, the setting of parameters for the controller is difficult since an accurate mathematical model is usually hard to obtain. It should be noted that a complex system is often composed with characteristics of non-linear, large time lag, uncertainty and time-variance. In this case it is impossible to obtain a precise mathematical model. An important branch of intelligent control, fuzzy logic control is an intelligent control method which uses fuzzy rule sets and linguistic representation of a human's knowledge to control a plant. The fuzzy logic technology has been widely applied in many control fields, and positive control effects have been obtained [14-20].

The essence of FLC is in converting expert knowledge of the related fields and the experience of skilled operators into language rules, implementing the complex system control by using fuzzy reasoning and fuzzy decision-making.

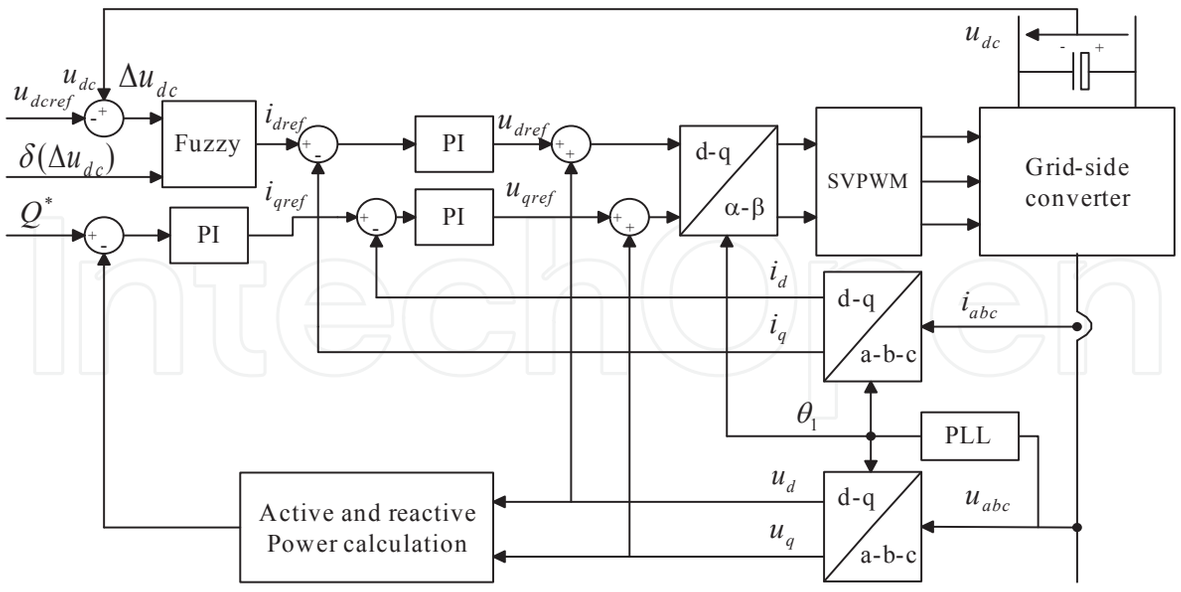

Figure 6. Direct fuzzy logic control strategy

In this part, three FLC-based control strategies are proposed for the DC-link voltage control to reduce the DC-link voltage ripples, where the PI controller is kept for the current inner loop and the controller of the outer loop is substituted by FLC in the double-closed loop control system of the WECS.

5.1. Direct FLC

Rule-based FLC is useful when the system dynamics are not well known or when they contain significant non-linearities, such as with wind containing large turbulence. FLC applies reasoning similarly to the way in which human beings make decisions; the controller rules thus contain expert knowledge of the system. The structure diagram of the direct FLC-based control strategy is shown in Figure 6.

The design process for a FLC consists of (i) determining the inputs, (ii) setting up the rules, and (iii) designing a method to convert the fuzzy result of the rules into output signal, known as defuzzification. The input and output membership functions are shown in Figure 7 and Figure 8, respectively. Triangular symmetrical membership functions are suitable for the input and output, which give more sensitivity especially as variables approach zero value. The width of variation can be adjusted according to the system parameters [15].

The proposed FLC method is based on the DC-link voltage deviation from the reference value Δu_{dc} and the variation $\delta(\Delta u_{\mathrm{dc}})$ during a sampled time; it is given as follows:

$$\begin{cases} \Delta u_{dc} = u_{dc} - u_{dcref} \\ \delta(\Delta u_{dc}) = \Delta u_{dc}(n) - \Delta u_{dc}(n-1) \end{cases} \tag{17}$$

http://dx.doi.org/10.5772/59923

where u_{dcref} is the referenced DC-link voltage.

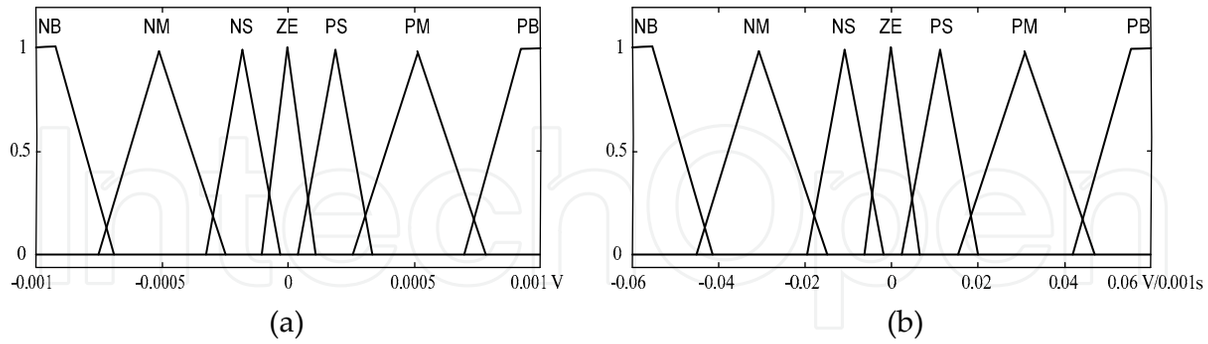

Figure 7. Membership functions of FLC: (a) input signal error of the DC-link voltage; (b) input signal variation of DC-link voltage

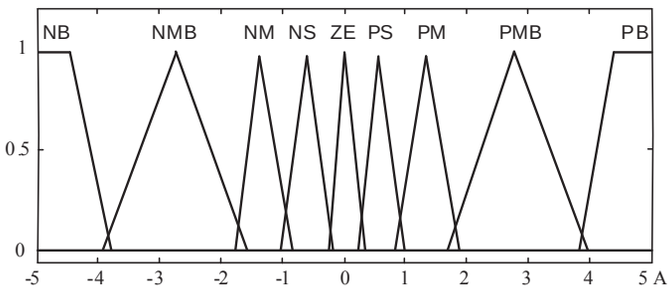

Figure 8. Membership function of output signal variation of reference d-axis current

In the proposed FLC system, nine fuzzy sets have been considered for variables: negative big (NB), negative medium big (NMB), negative medium (NM), negative small (NS), zero (ZE), positive small (PS), positive medium (PM), positive medium big (PMB), and positive big (PB). The rules of the FLC are shown in Table 1.

$\delta\Delta u_{dc}$	Δu_{dc}						
	NB	**NM**	**NS**	**ZE**	**PS**	**PM**	**PB**
NB	NB	NMB	NM	NM	NS	NS	ZE
NM	NMB	NM	NM	NS	NS	ZE	PS
NS	NM	NM	NS	NS	ZE	PS	PS
ZE	NM	NS	NS	ZE	PS	PS	PM
PS	NS	NS	ZE	PS	PS	PS	PM
PM	NS	ZE	PS	PS	PM	PM	PMB
PB	ZE	PS	PS	PM	PM	PMB	PB

Table 1. Rules of the FLC

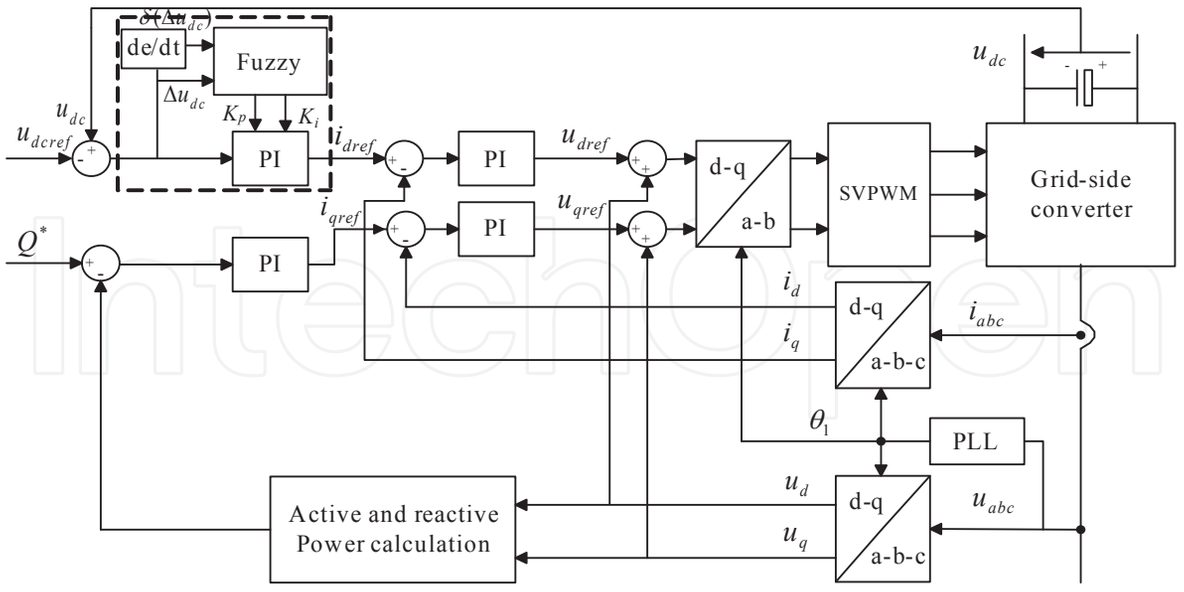

Figure 9. Fuzzy-adaptive-PI-based vector control strategy

5.2. Fuzzy adaptive PI control

Based on new theory and new technology, fuzzy adaptive control is an effective method to solve the problem of PI parameters' online self-tuning. The idea of fuzzy adaptive PI control is combines a conventional PI controller with FLC. On the one hand, it has adaptive ability, which enables it to automatically identify the controlled process parameters, set control parameters, and adapt to the changes of process parameters. On the other hand, it also has the advantages of the PI controller, such as simple structure, high reliability and familiarity to practical engineering-design personnel [21-26].

The block diagram of fuzzy adaptive PI control is shown in Figure 9. The DC-link voltage control loop consists of one conventional PI controller and one online fuzzy inference calculation. The calculation part is actually a FLC. The PI parameters are modified online by using the fuzzy rules, and then the fuzzy adaptive PI controller is constructed.

The design process for a fuzzy adaptive PI controller consists of four parts: (i) determining of inputs and outputs, (ii) reasoning of fuzzification and fuzzy logic, (iii) defuzzification, (iv) parameters' online self-tuning of PI controller.

a. *Inputs and outputs determining*

The inputs of the FLC are the deviation e (e=U_{dcref}-u_{dc}) and the rate of the deviation e_c. The inputs are continuously checked and calculated by the FLC, and then the parameters of the PI controller are adjusted online by using the fuzzy logic rules in order to achieve optimal parameters. As the inputs of FLC in fuzzy adaptive PI controller, error e and error change rate e_c can satisfy the requirements of PI parameters' self-tuning at different times.

The input signals have seven membership functions, while the outputs each have seven membership functions. The design of the input membership functions of variables is shown

http://dx.doi.org/10.5772/59923

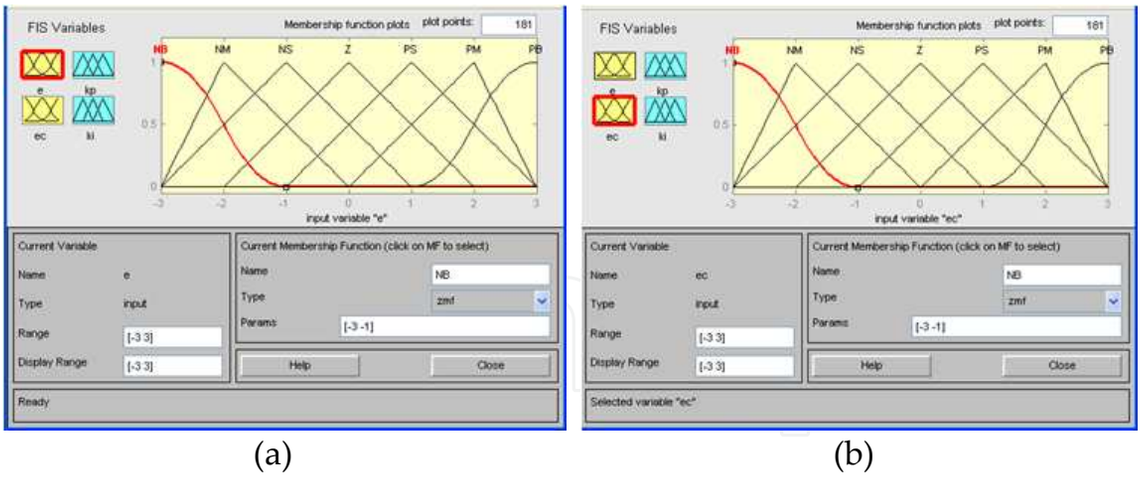

Figure 10. Input membership functions of fuzzy language variables (a) e (b) e_c

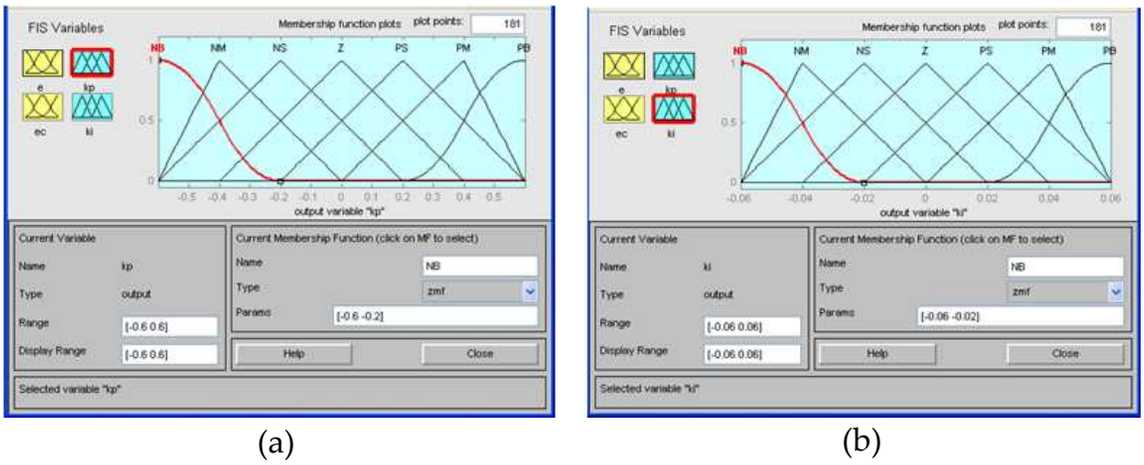

Figure 11. Output membership functions of language variables (a) ΔK_P (b) ΔK_i

in Figure 10. The membership functions of the proportional gain K_p and the integral gain K_i are designed as shown in Figure 11.

The fuzzy set domain ranges of input and output variables are obtained by simple calculation of normalization. The fuzzy set domain of input variables are set as $e,\ ec=\{-3,\ -2,\ -1,\ 0,\ 1,\ 2,\ 3\}$ and the fuzzy set domain of outputs $\Delta K_{P,}\ \Delta K_i$ are set as (-0.6, 0.6) and (-0.06, 0.06) respectively.

The corresponding fuzzy sets of input and output variables are set as

$$e, e_c, \Delta K_P, \Delta K_i = \{NB, NM, NS, Z, PS, PM, PB\} \tag{18}$$

where negative big (NB), negative medium (NM), negative small (NS), zero (Z), positive small (PS), positive medium (PM), positive big (PB) refer to the fuzzy sets' means.

b. *Fuzzification and fuzzy reasoning*

All the fuzzy variables obey the normal distribution. The fuzzy inference system uses Mamdani type, as follows:

$$If\ e\ is\ A\ and\ e_c\ is\ B,\ then\ u\ is\ c$$

The fuzzy logic rules of the output variables are shown in Table 2 and Table 3, respectively.

e	e_c						
	NB	**NM**	**NS**	**Z**	**PS**	**PM**	**PB**
NB	PB	PB	PM	PM	PS	Z	Z
NM	PB	PB	PM	PS	PS	Z	NS
NS	PM	PM	PM	PS	Z	NS	NS
Z	PM	PM	PS	Z	NS	NM	NM
PS	PS	PS	Z	NS	NS	NM	NM
PM	PS	Z	NS	NM	NM	NM	NB
PB	Z	Z	NM	NM	NM	NB	NB

Table 2. Fuzzy logic rules of ΔK_P

e	e_c						
	NB	**NM**	**NS**	**Z**	**PS**	**PM**	**PB**
NB	NB	NB	NM	NM	NS	Z	Z
NM	NB	NB	NM	NS	NS	Z	Z
NS	NB	PM	NS	NS	Z	PS	PS
Z	NM	NM	NS	Z	PS	PM	PM
PS	NM	NM	Z	PS	PS	PM	PB
PM	Z	Z	PS	PS	PM	PB	PB
PB	Z	Z	PS	PM	PM	PB	PB

Table 3. Fuzzy logic rules of ΔK_i

c. *Defuzzification*

Defuzzification involves designing a method to convert the fuzzy results of the rules into output signals. The weighted average method is adopted to obtain accurate FLC output. The weighted average method is described as follows:

http://dx.doi.org/10.5772/59923

$$u_0 = \frac{\sum_{i=1}^{n} u_i \mu_c(u_i)}{\sum_{i=1}^{n} \mu_c(u_i)} \tag{19}$$

d. *Parameters' online self-tuning of PI controller*

The proposed PI parameters' self-tuning seeks to find out the fuzzy relationship between two parameters of PI and the inputs of FLC. In order to implement the FLC algorithm of the grid connected in a closed loop, the DC-link voltage u_{dc} is sensed and then compared with the reference DC-link voltage U_{dcref}. In order to meet the control parameters of different requirements for different e and e_c, the deviations e and e_c are continuously checked and calculated by the FLC, and then the parameters of the PI controller are adjusted online by using the fuzzy rules in order to achieve an excellent dynamic and static performance of the WECS. Parameters' self-tuning is based on fuzzification results processing, fuzzy reasoning and defuzzification. In order to achieve the purpose of online regulation, the work flowchart of parameters' online regulation is given in Figure 12.

The parameter regulation formula of the PI controller is

$$\begin{cases} K_p = K_p^* + \Delta K_p \\ K_i = K_i^* + \Delta K_i \end{cases} \tag{20}$$

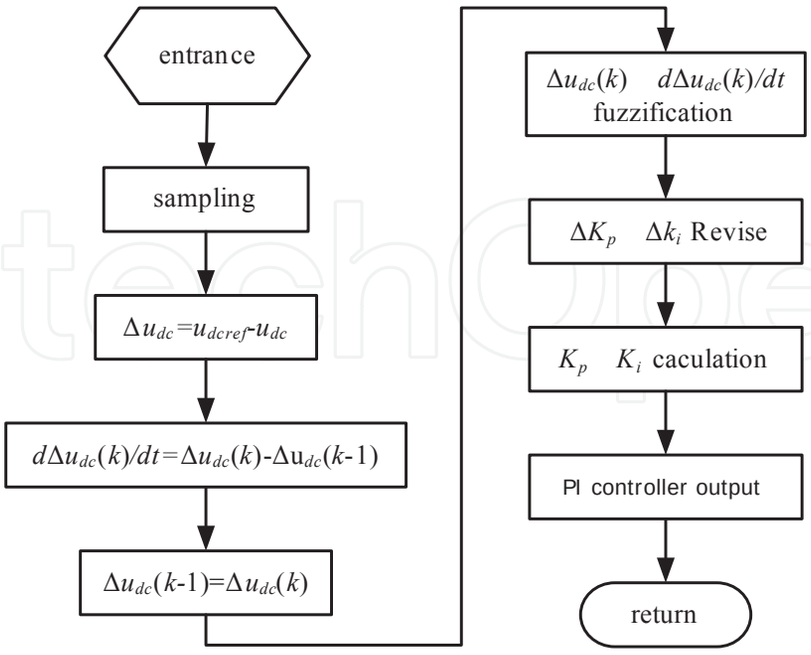

Figure 12. The flow chart of parameters' online regulation

5.3. Double-loop FLC

The block diagram of the double-loop fuzzy logic control strategy is shown in Figure 13. As with the previous FLC control strategies, the outer control loop of the DC-link voltage is substituted. The structure of the double-loop control scheme is shown in Figure 14.

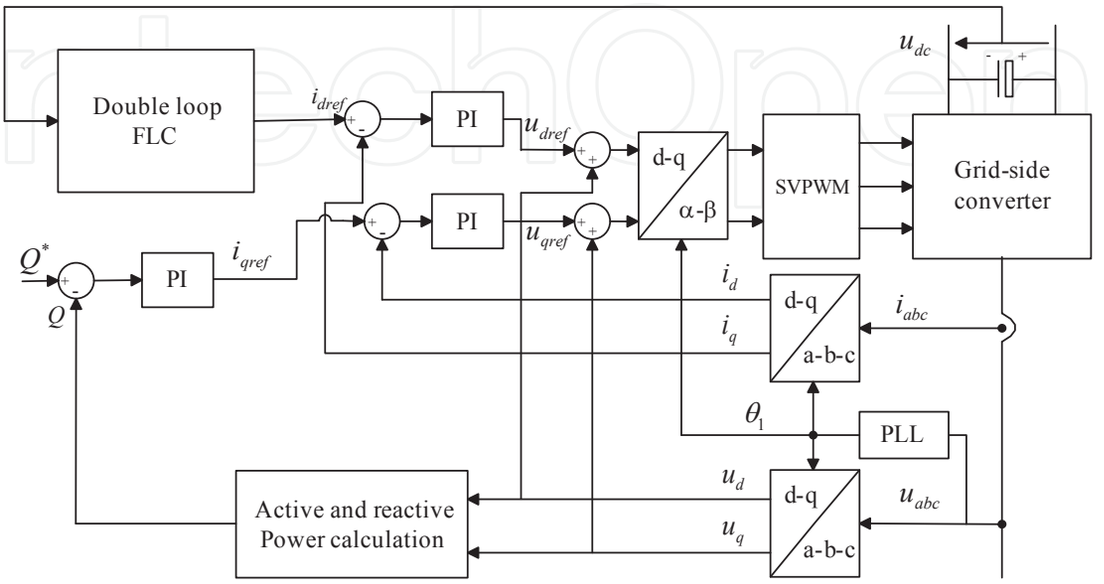

Figure 13. Double-loop fuzzy logic control strategy

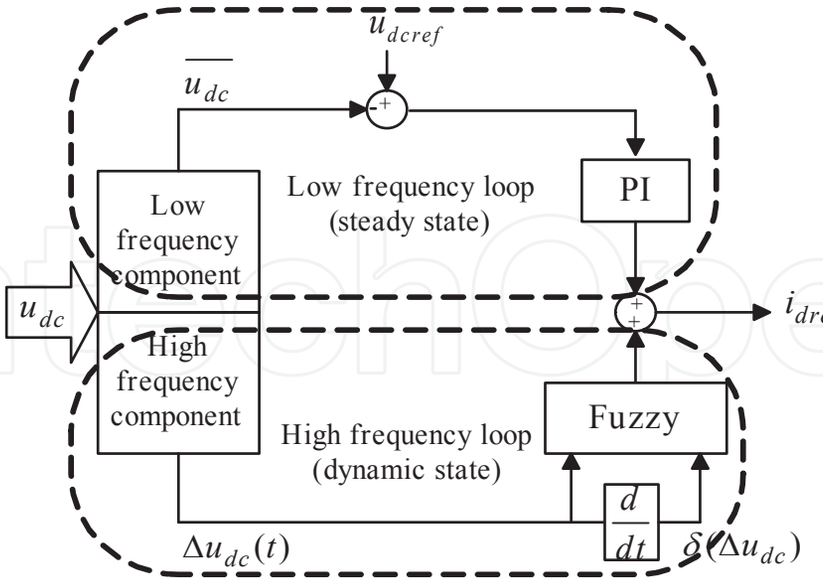

Figure 14. Double-loop control scheme for variable-speed WECS

It can be seen that the control system is divided into low-frequency and high-frequency loops. The low-frequency loop typically incorporates the slow variation of the wind energy, and its

http://dx.doi.org/10.5772/59923

task is to track the optimal operating point. The high-frequency loop utilizes small-signal perturbations about the operating point, determined by the low-frequency loop. The high-frequency loop captures the transient behaviour excited by the high-frequency and turbulent component of the wind.

The FLC is applied in the high-frequency loop to eliminate or reduce the dynamic error of the DC-link voltage due to the dynamic characteristics of the WECS. The inputs of the FLC are the deviation of DC-link voltage (Δu_{dc}) and the rate of the deviation $\delta(\Delta u_{dc})$. Meanwhile, the PI controller is used to eliminate static error between the average DC-link voltage and the reference DC-link voltage. Then, the steady-state characteristics of the system can be improved. The double-loop FLC can reduce the ripples of the DC-link voltage significantly and improve the performances of the WECS. In this case a smaller capacitor may be used for the DC link and a more compact WECS may be achieved.

6. Simulations

In order to verify the effectiveness of the proposed control strategies and evaluate the performance of the control system, a simulation model of WECS is constructed by using the MATLAB/Simulink tool. The simulation model of the WECS is shown in Figure 15.

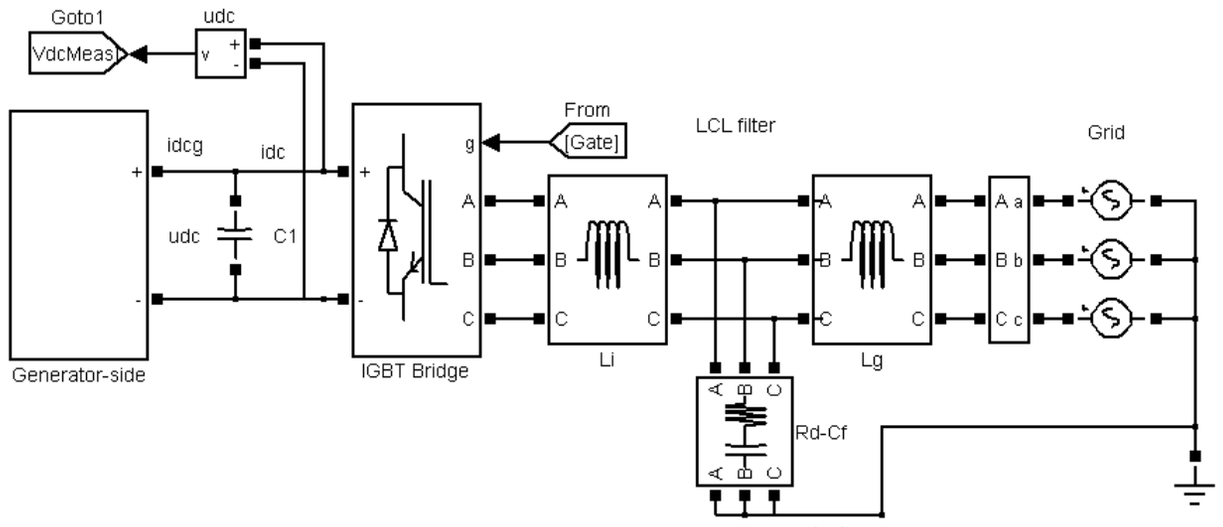

Figure 15. Simulation model of the WECS

The wind model is essential to obtain realistic simulations of the power fluctuations in the power production of the wind turbines. Hence, to investigate the steady-state and transient performance of the controller under different circumstances, different wind models are studied, namely a step wind model and a stochastic wind model.

At low wind-speed below the rated condition, the PM generator is supposed to work in an MPPT strategy. For a well designed generator-side control system, a simple model for the

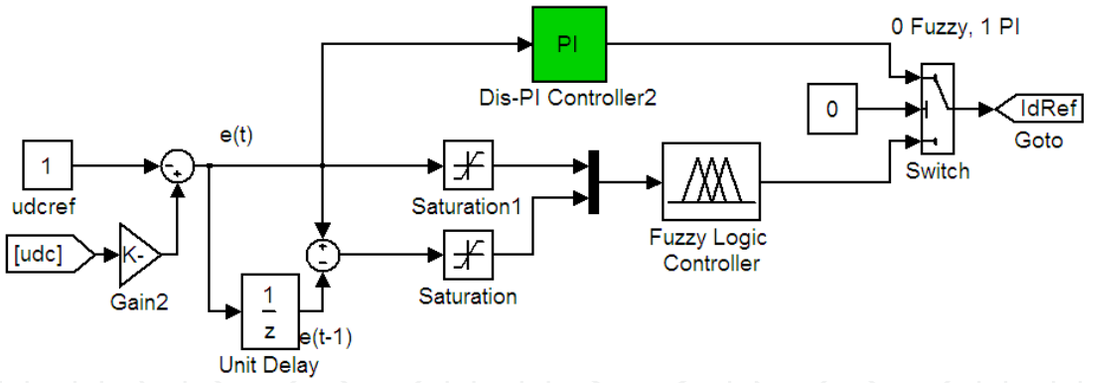

Figure 16. Simulation model of direct FLC with PI controller

generator-side converter may be used where the electrical power injected to the DC link is proportional to the cube of the wind-speed. The parameters of the proposed PM generation system are shown in Table 4.

Parameters	Values
Rated power	3000 W
Rated line to line voltage	380 V/50 Hz
LCL filer	L_g=3.4 mH, L_i=6.9 mH, C_f=2.04 μF, R_d=11 Ω
DC-link capacitor	390 μF
Outer-loop PI controller	k_p=40, k_i=150
Inner-loop PI controller	k_p=0.2, k_i=250

Table 4. Parameters of the proposed PM generation system

6.1. Simulation results of direct FLC

The model of FLC is shown in Figure 16, where the PI controller is also included for comparison. By changing the value of the switch, one of the FLC and PI controllers may be selected.

a. *Step wind model*

The injected current i_{dcg} of the step wind model is shown in Figure 17, where the initial current is 2.14 A and the final current is 4.28 A. The simulation results are shown in Figure 18 and Figure 19.

Figure 18 shows the results of the PI controller, where much large DC-link voltage fluctuation can be seen. The dynamic adjust time of the PI controller is much longer than that of the direct FLC. The results in Figure 19 reveal nearly no voltage fluctuation, and that the voltage ripple is reduced significantly.

http://dx.doi.org/10.5772/59923

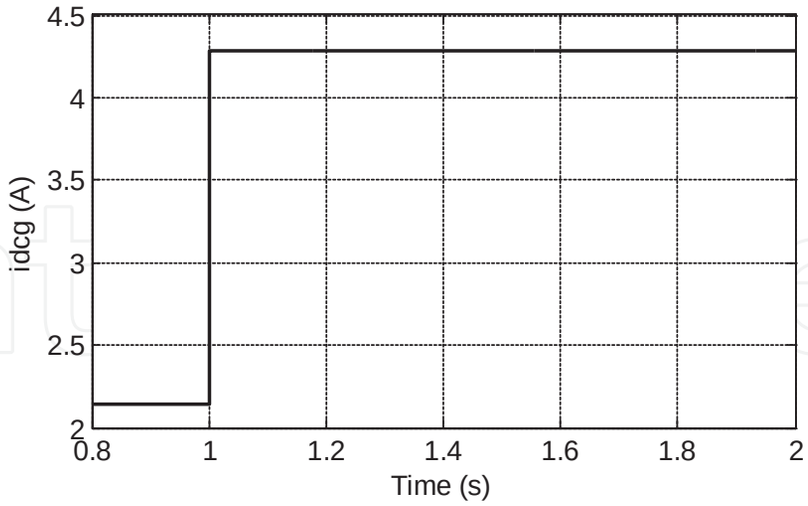

Figure 17. Step wind injection model

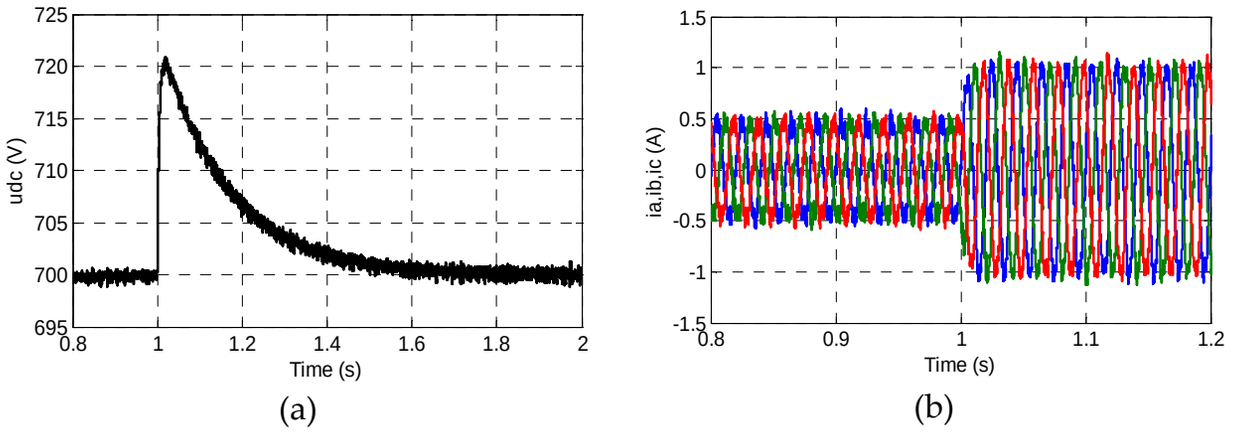

Figure 18. Simulation results of step wind model for PI controller: (a) DC-link voltage variations; (b) grid-side currents.

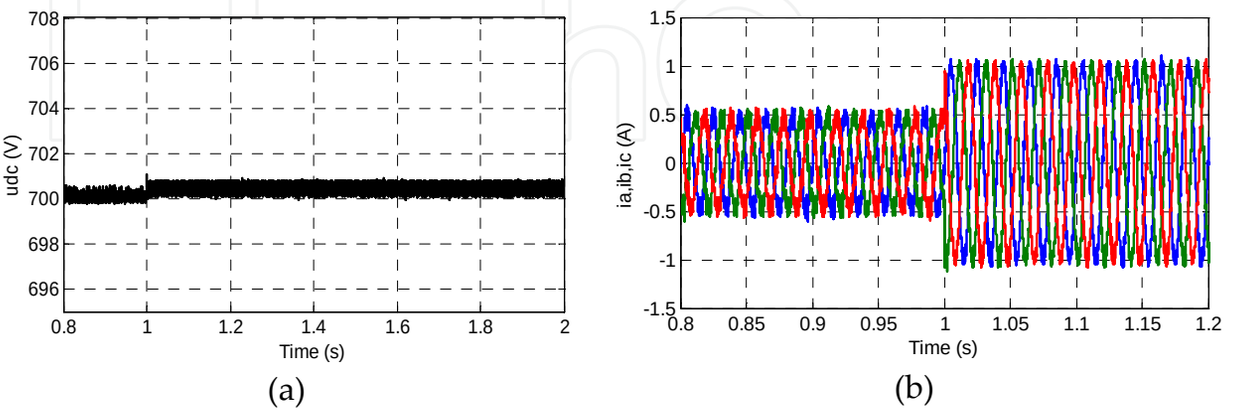

Figure 19. Simulation results of step wind model for direct FLC: (a) DC-link voltage variations; (b) grid-side currents.

b. *Stochastic wind model*

The stochastic wind model is shown in Figure 20(a) and the injected current is shown in Figure 20(b). In order to observe the DC-link voltage fluctuations, the simulation time is set to only two seconds. The simulation results of the PI controller and FLC are shown in Figure 21 and Figure 22, respectively, where larger voltage variations are shown for the PI controller than for the FLC.

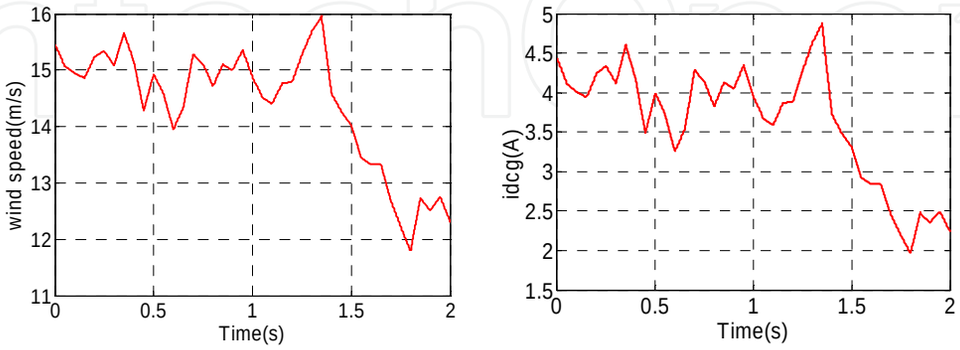

Figure 20. Stochastic wind model: (a) wind-speed; (b) injected current to DC-link

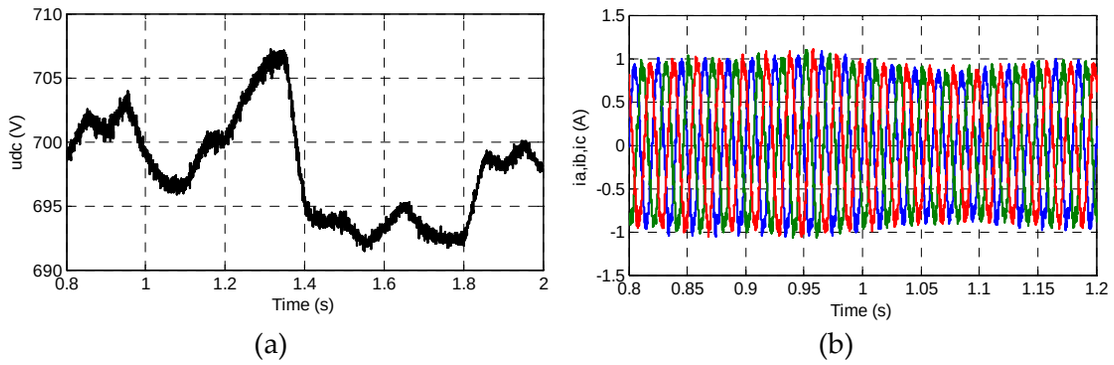

Figure 21. Simulation results of stochastic wind model for PI controller: (a) DC-link voltage variations; (b) grid-side currents.

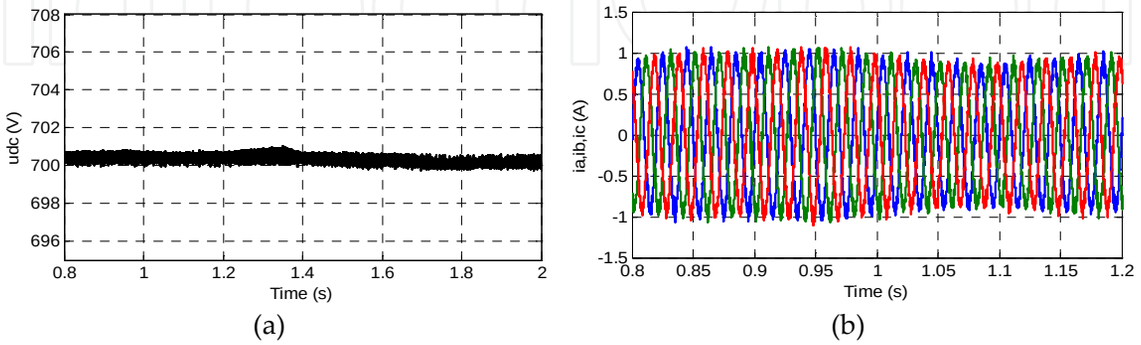

Figure 22. Simulation results of stochastic wind model for direct FLC: (a) DC-link voltage variations; (b) grid-side currents.

http://dx.doi.org/10.5772/59923

The comparisons of the DC-link voltage ripples are shown in Table 5, where the DC-link voltage ripple is expressed as $\Delta u_{dc}/u_{dc}$.

Wind model	DC-link voltage ripples $\triangle u_{dc}/u_{dc}$(%)	
	PI controller	Direct FLC
Step wind	2.86	0.17
Stochastic wind	2.0	0.16

Table 5. Comparisons of the DC-link voltage ripples

According to the injected wind model simulation, it is shown that the FLC has less voltage fluctuation and ripples than the PI controller. This will improve the dynamic performance of the WECS. Considering all the stochastic natural wind, the FLC seems much more suitable for the DC-link voltage control in the wind power generation system than the traditional PI controller. It should be noted that the simulation time is limited to two seconds for stochastic wind model. However, according to the van der Hoven wind spectrum, wind turbulence can occur on the level of tenths of seconds to several minutes. So, the DC-link voltage ripples may be increased a little both for the PI controller and the FLC, if the longer simulation time is used.

6.2. Simulation results of fuzzy adaptive PI controller

The simulation model of fuzzy adaptive PI controller is shown in Figure 23. Firstly, the fuzzy adaptive PI controller and PI controller are compared under the same wind model conditions as are shown in Figure 20.

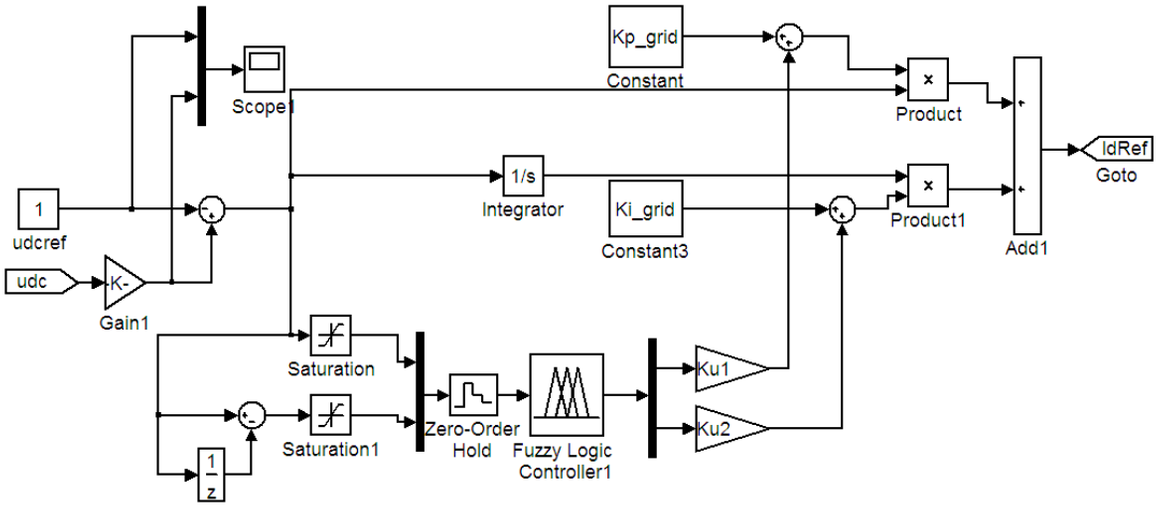

Figure 23. Simulation model of fuzzy adaptive PI controller

The DC-link voltage variations under the PI control and the fuzzy adaptive PI control are shown in Figures 24(a) and 24(b), respectively. It can be seen that the DC-link voltage is fluctuated with the same tendency according to the stochastic wind, and the voltage ripples

are very large. The fuzzy adaptive PI controller can restrain the fluctuation and reduce the voltage ripples effectively.

In order to investigate the transient performance and robustness of the fuzzy adaptive PI controllers, simulations with dynamically injected wind energy are carried out.

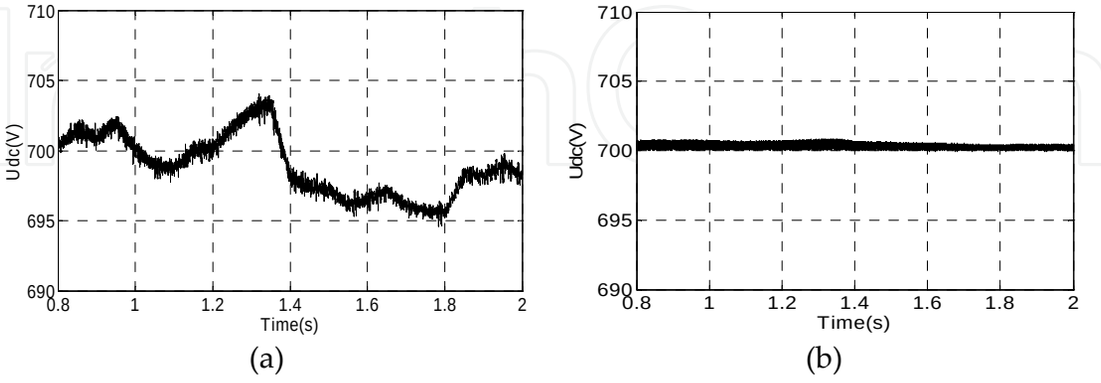

Figure 24. DC-link voltage variations: (a) with PI controller; (b) with the fuzzy adaptive PI controller

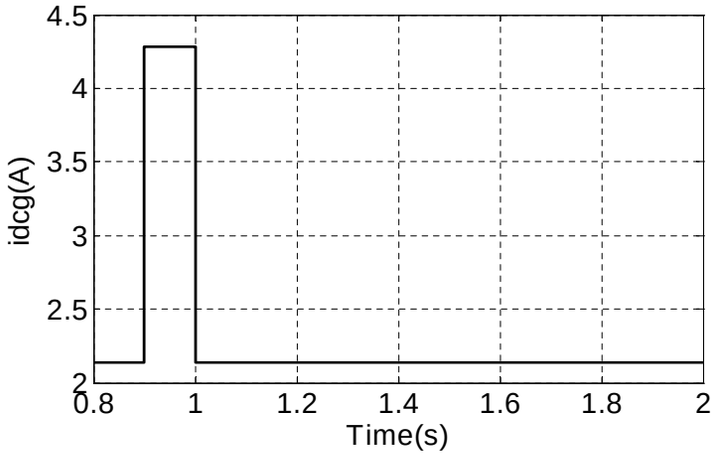

Figure 25. The current injected into the DC link

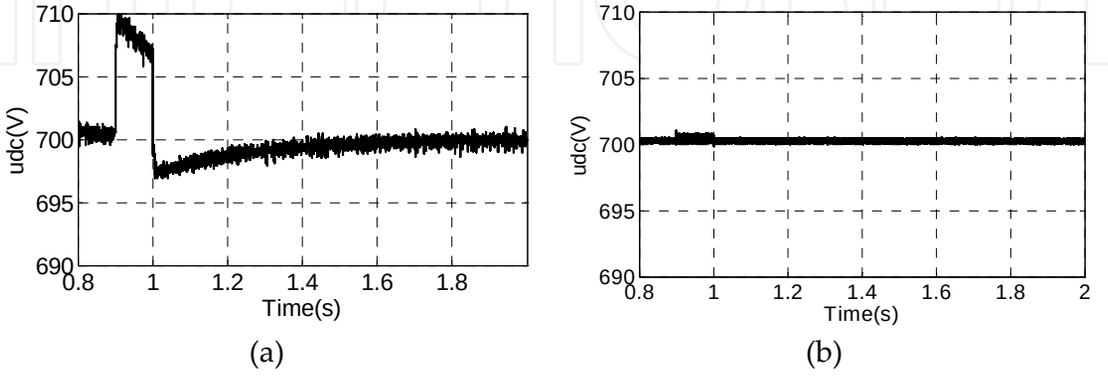

Figure 26. DC-link voltage variations: (a) with PI controller; (b) with fuzzy adaptive PI controller

http://dx.doi.org/10.5772/59923

Figure 25 shows a current suddenly injected into the DC-link at 0.8 to 0.9 seconds. In this case a sudden jump of DC-link voltage occurs in the PI control system, as shown in Figure 26(a). However, only very small fluctuation is seen in this period for the fuzzy adaptive PI controller, as shown in Figure 26(b). The DC-link voltage under fuzzy adaptive PI control has very little ripples and the adjust time is very fast, meaning the WECS has quick dynamic response and good transient performance. Figure 27 shows the three-phase grid-side current with PI controller and fuzzy adaptive PI controller, respectively.

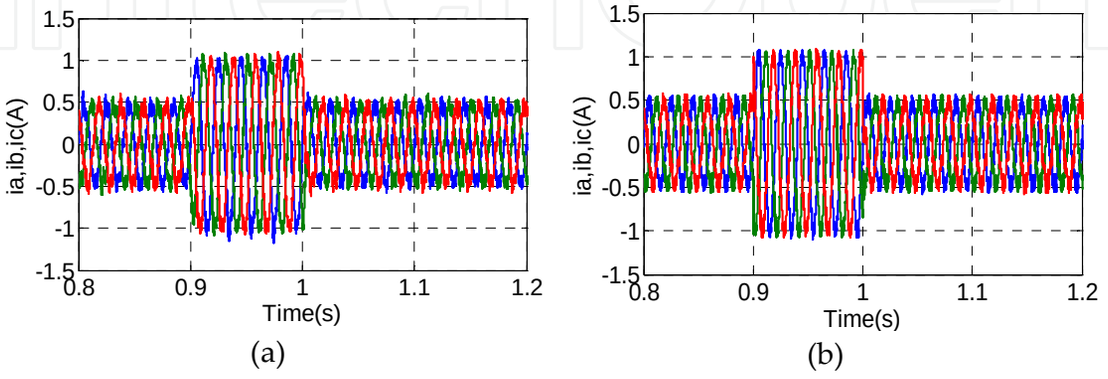

Figure 27. Three-phase grid-side current: (a) with PI controller; (b) with fuzzy adaptive PI controller

It can be seen in the simulation results that the fuzzy adaptive PI controller shows better performance than the PI controller. The performance might be improved by adjusting the parameters of the PI controller. However, it is hard to balance the overshoot and dynamic response at the same time. By incorporating the PI with the FLC, namely the fuzzy adaptive PI, the transient adjustment time is decreased significantly and the overshoot is greatly reduced through online self-tuning of the parameters of the PI controller.

6.3. Simulation results of double-loop FLC

The simulation model of the double-loop FLC is shown in Figure 28. Here a mean block is designed to obtain the component of the low-frequency loop.

Firstly, the double-loop FLC and the PI controller are compared under the conditions of the stochastic wind model. The injected current of the stochastic wind model is shown in Figure 20. The DC-link voltage variations under certain wind models are simulated and the results show that large DC-link voltage ripples are obtained with the PI controller, while the DC-link voltage hardly fluctuates in double-loop FLC, as shown in Figure 29.

In order to investigate the transient performance of the proposed double-loop FLC, the stochastic wind model with step mean wind-speed at 1.0 seconds is simulated, as shown in Figure 30. The mean wind-speed is 13 m/s during the period 0~1 seconds and 7 m/s during the period 1~2 seconds. Figure 31 shows the simulation results under the stochastic wind model. The DC-link voltage shows a negative jump at 1.0 seconds in the case of the PI controller, while in the case of double-loop FLC, DC-link voltage fluctuation is hardly observed.

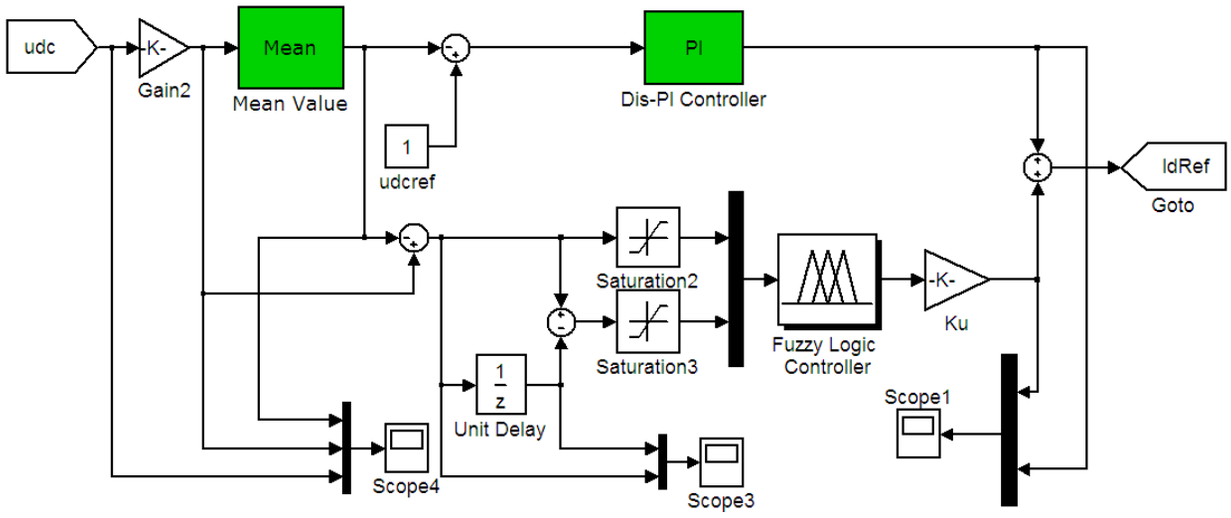

Figure 28. Simulation model of double-loop FLC

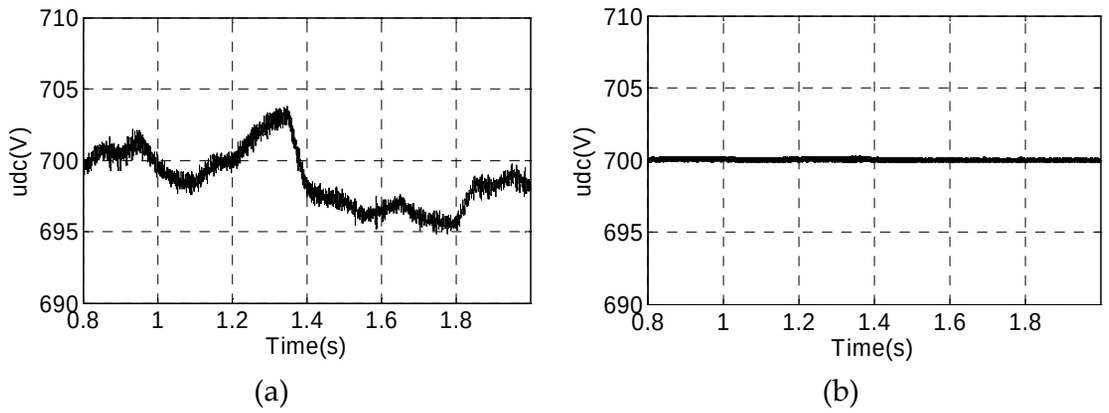

Figure 29. DC-link voltage variations: (a) with PI controller; (b) with double-loop FLC

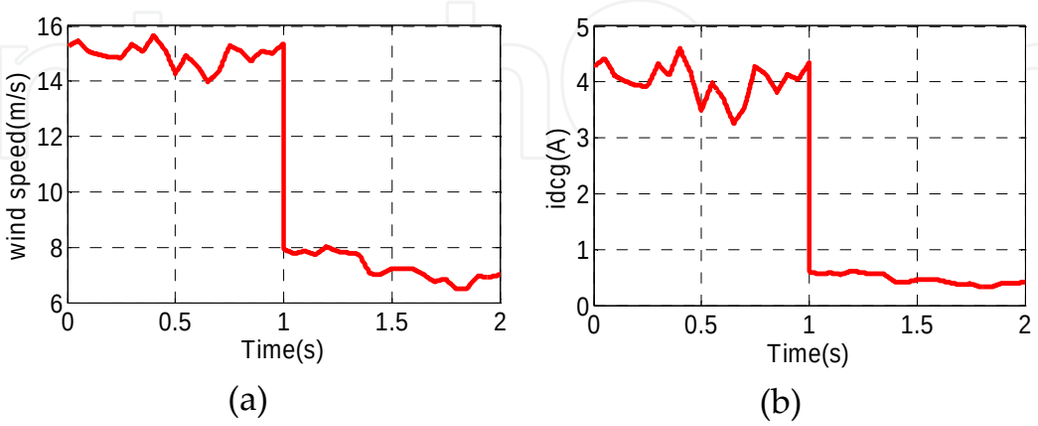

Figure 30. Stochastic wind model of double-loop FLC: (a) wind-speed; (b) injected current

http://dx.doi.org/10.5772/59923

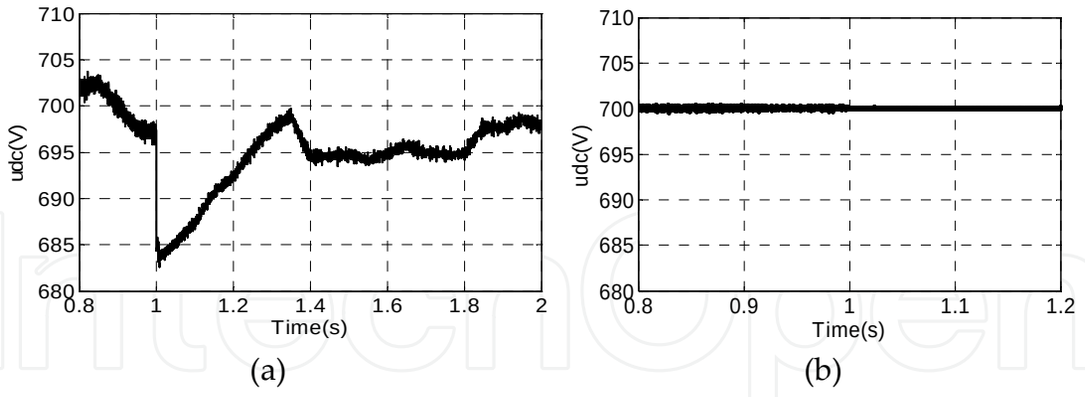

Figure 31. DC-link voltage variations: (a) with PI controller; (b) with double-loop FLC

6.4. Comparisons of fuzzy based control strategies

Three FLC-based control strategies are simulated and compared with the traditional PI controller. Simulation results reveal that the FLC-based controllers have a better dynamic response. In this part, three fuzzy-based control strategies are simulated and compared with each other under different wind models.

a. *Step wind model*

The same step wind injection model as shown in Figure 17 is used for FLC-based controllers. The simulation results are given in Figure 32. It is shown in Figure 32(b) that the fuzzy adaptive PI has the largest voltage overshoot. This is because the adaptive PI controller is essentially a PI regulator. Similar characteristics of the PI controller are seen in the fuzzy adaptive PI controller. However, the dynamic-response performance is greatly improved by the FLC loop, which is shown in Figure 32. The dynamic regulation time is short in all the fuzzy-based control strategies. It should be noted that steady error exists for direct FLC, as shown in Figure 32(a), where the voltage in infinite time is not the same as in the time before disturbance occurring.

Compared with the direct FLC, the double-loop FLC has the least voltage overshoot, as shown in Figure 32(c), which makes it the most ideal control strategy for the WECS. However, the double-loop FLC also has a more complicated structure and more complicated algorithms than the direct FLC.

b. *Sudden injected energy*

The performances of the FLC-based control strategies are compared under sudden injected energy. Figure 33 shows the injected current to the DC-link due to supposed sudden wind changes, where two cases, namely sudden positive and sudden negative injected current, are considered. The simulation results are presented in Figure 34 to Figure 36. It is shown that both the injected energy disturbances at 0.9 to 1.0 seconds lead to a dynamic process for the three FLC-based control strategies, where the direct FLC has the poorest performance. The latter

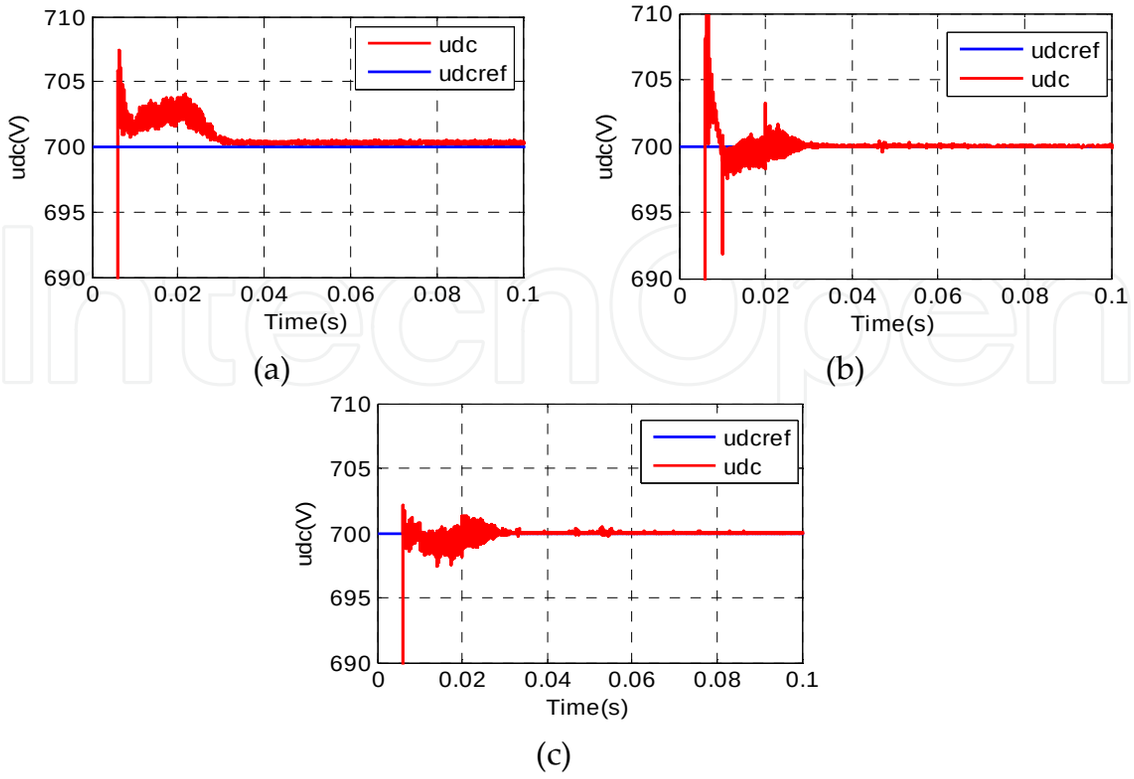

Figure 32. Simulation results of step wind model: (a) with direct FLC; (b) with fuzzy adaptive PI controller; (c) with double-loop FLC

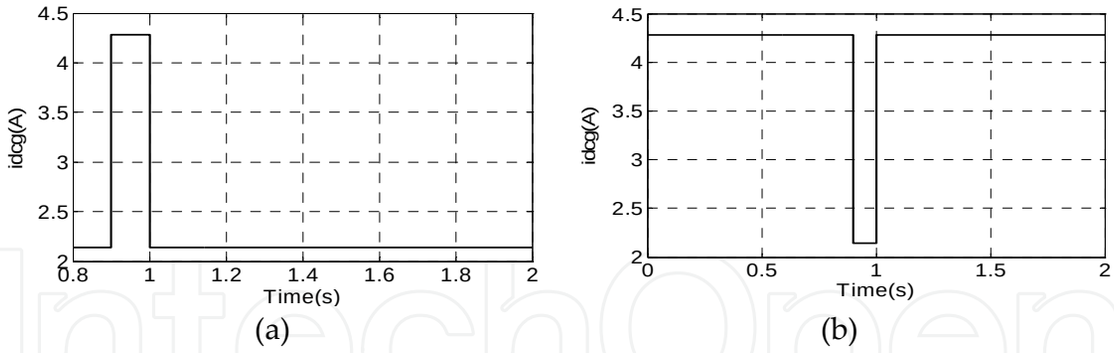

Figure 33. The injected current to the DC-link; (a) positive; (b) negative

control strategies, namely fuzzy adaptive PI and double-loop FLC, have nearly the same DC-link voltage ripples during the simulation; however, the double-loop FLC has smaller steady voltage error in the disturbance period.

c. *Stochastic wind model*

Figure 37 shows the injected current of a stochastic wind model with mean wind-speed 7 m/s. The simulation results are presented in Figure 38. Similar results may be obtained where the dynamic DC-link voltage fluctuation is large for the direct FLC. Furthermore, the direct

http://dx.doi.org/10.5772/59923

FLC has the largest steady voltage errors during the whole simulation period. Considering the voltage fluctuations between the fuzzy adaptive PI and the double-loop FLC, the latter shows slightly better performances.

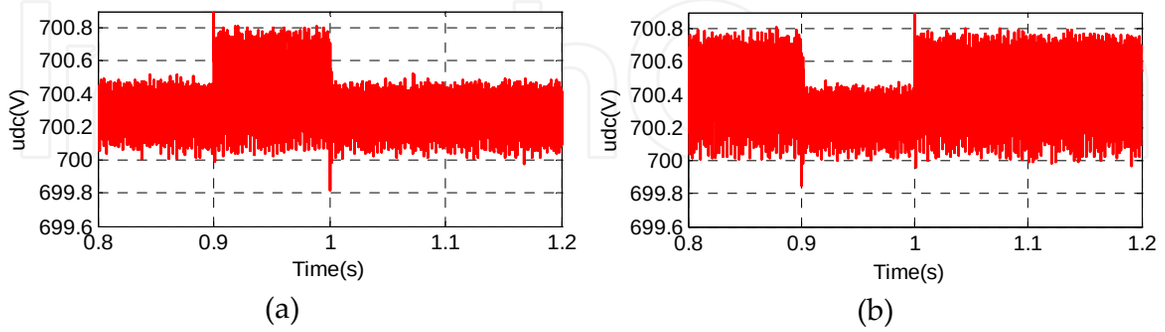

Figure 34. DC-link voltage variations with direct FLC: (a) positive; (b) negative

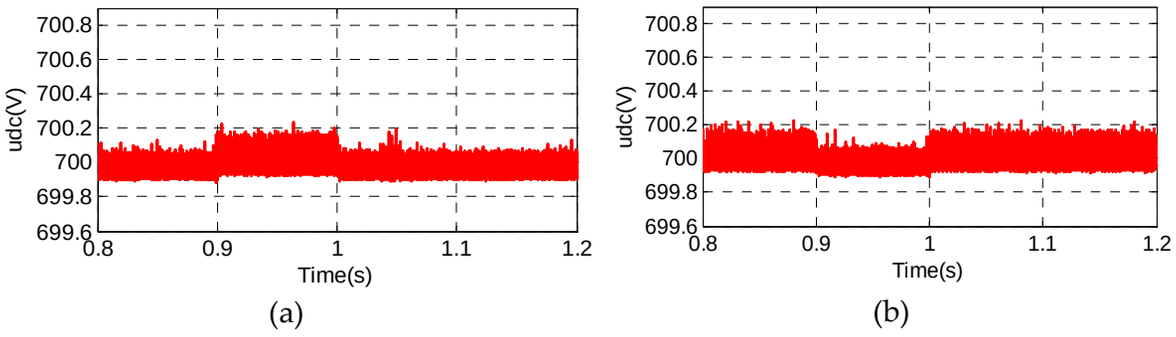

Figure 35. DC-link voltage variations with fuzzy adaptive PI controller: (a) positive; (b) negative

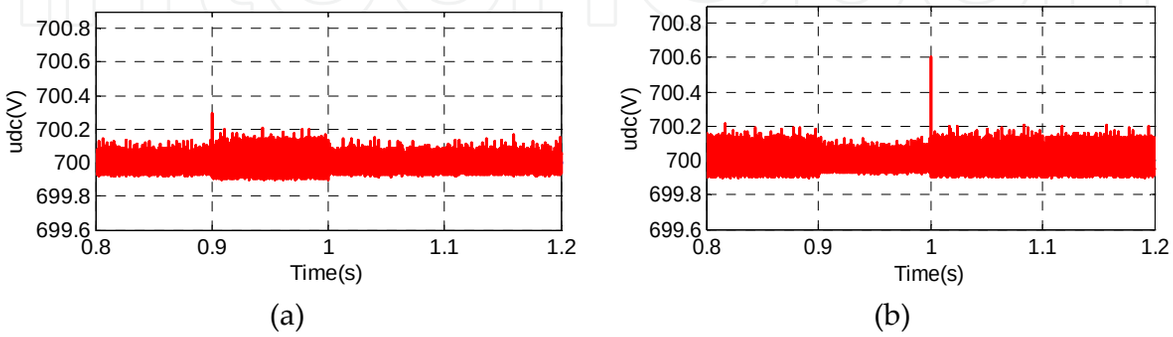

Figure 36. DC-link voltage variations with double-loop FLC (a) positive; (b) negative

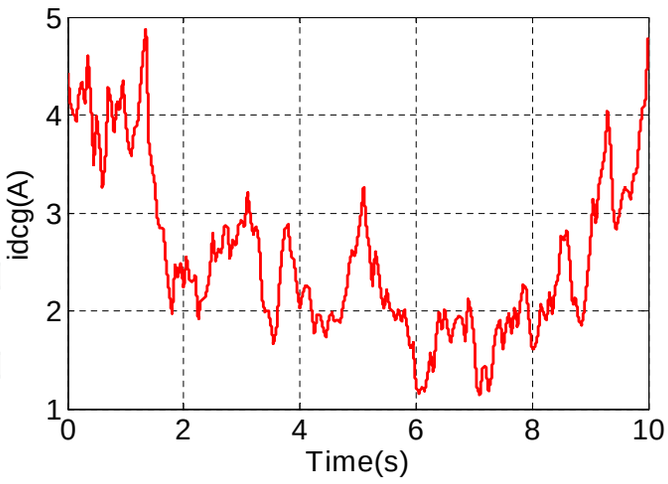

Figure 37. Injected current of stochastic wind model

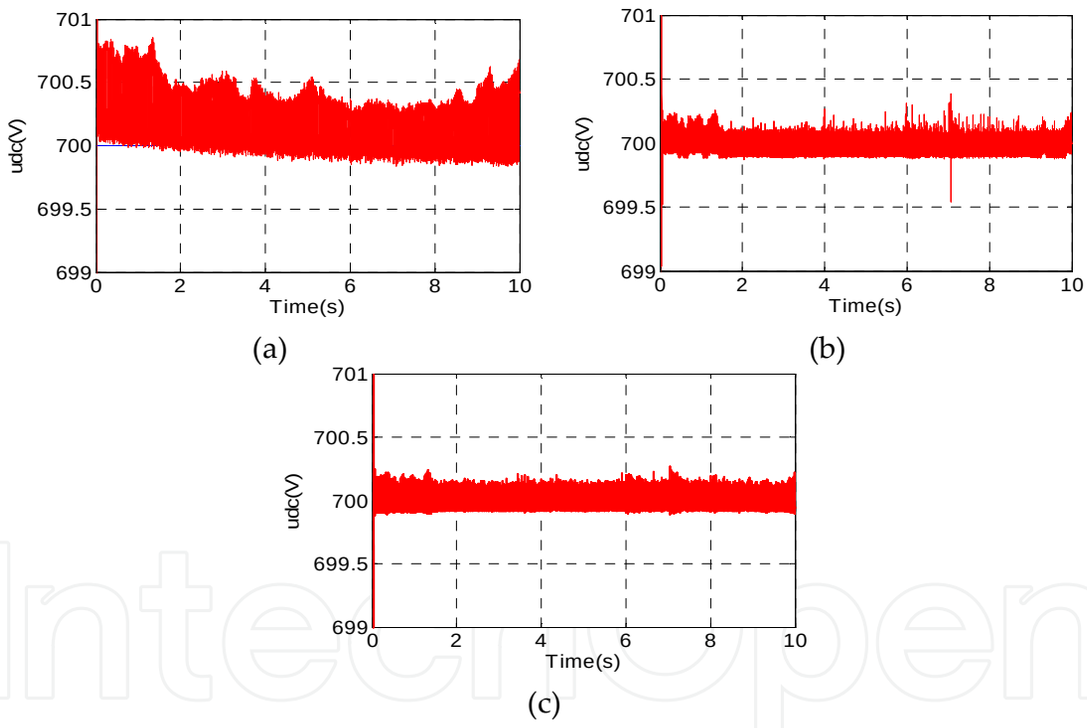

Figure 38. Simulation results of (a) direct FLC; (b) fuzzy adaptive PI controller; (c) double-loop FLC

7. Conclusions

The turbulence of the wind model will result in dynamic power variations and increase the DC-link voltage ripples, which will deteriorate the grid-side power quality. The traditional PI control strategy is discussed and three fuzzy-based control strategies for DC-link voltage

control are proposed in this chapter. The simulation models are constructed in a MATLAB/Simulink surrounding and simulations and comparisons between the different control strategies are carried out, where different wind models are used.

The simulation results show that the three fuzzy-based control strategies have better dynamic- and steady-state performances than the traditional PI controller when the stochastic wind model is considered. Due to the good dynamic and robustness of fuzzy logic control, the fuzzy-logic-based control strategies may be much more suitable for DC-link voltage control in the WECS than the traditional PI controller. Considering only the fuzzy-based controller, the fuzzy adaptive PI controller has the largest voltage overshoot during the disturbance, while the dynamic adjustment time is as short as other FLC. The direct FLC has small steady error under disturbance while the fuzzy adaptive PI and double-loop FLC have none. Since the double-loop FLC has fast dynamic response, limited voltage overshoot, and small DC-link voltage ripples in the stochastic wind model, it is supposed as the best choice for the DC-link voltage control of the WECS. However, the double-loop FLC has more complicated structure and algorithms than the direct FLC.

Acknowledgements

This work was supported by a grant of the National Nature Science Foundation of China (51137001, 51320105002) and a grant of the Prospective Joint Research Project of Jiangsu Province under Project No. BY2013073-05.

Author details

Jianzhong Zhang* and Shuai Xu

*Address all correspondence to: jiz@seu.edu.cn

School of Electrical Engineering, Southeast University, Nanjing, China

References

[1] Heier S. Grid integration of wind energy conversion systems. 2nd Edition, translated by Rachel Waddington, John Wiley & Sons, Ltd., Chichester UK, 2006.

[2] Li J, Cai F, Qiao L, et al. Annual review and outlook on China wind power. CWEA, Beijing, China, 2013.

[3] Zhang J, Cheng M, Chen Z. Nonlinear control for variable-speed wind turbines with permanent magnet generators. Proceedings of International Conference on Electrical Machines and Systems, Seoul, Korea, 2007, pp. 24-329.

[4] Chinchilla M, Arnaltes S, Burgos J. C. Control of permanent-magnet generators applied to variable-speed wind-energy systems connected to the grid. IEEE Transactions on Energy Conversion 2006; 21(1): 130-135.

[5] Abo-Khalil A. G, Lee D, Seok J. Variable speed wind power generation system based on fuzzy logic control for maximum output power tracking. 35th Annual IEEE Power Electronics Specialists Conference, Achen, Germany, 2004.

[6] Muljadi E, Pierce K, Migliore P. Control strategy for variable-speed stall-regulated wind turbines. American Controls Conference, Philadelphia, USA, 1998, pp. 1-5.

[7] Zhang J, Cheng M. DC Link Voltage Control Strategy of Grid-connected Wind Power Generation System. 2nd IEEE International Symposium on Power Electronics for Distributed Generation Systems, Hefei, China, 2010, pp. 970-975.

[8] Silva N, Martins A, Carvalho A. Design and evaluation of a PWM rectifier control system for testing renewable DC sources connected to the grid. Inter. SPEEDAM 2006, Taormina, Italy, 2006, pp. 32-37.

[9] Sastry J, Ojo O, Wu Z. High-performance control of a boost AC-DC PWM rectifier/ induction generation system. IEEE Trans. on Ind. Appli. 2006; 42(5): 1146-1154.

[10] Skretas S. B, Papadopoulos D. P. Enhance design and performance of WECS with PMSG connected to MV grid using intelligent control methods. Proc. of the 2008 International Conference on Electrical Machines, Vilamoura, Portugal, 2008.

[11] Chen Y. M, Cheng C. S, Wu H. C. Grid-connected hybrid PV/wind power generation system with improved DC bus voltage regulation strategy. APEC 2006, Dallas Texas, 2006, pp. 1088-1094.

[12] Liu Z, Liu B, Duan S, and Kang Y. A novel DC capacitor voltage balance control method for cascade multilevel STATCOM. IEEE Trans. Power Electron, Jan. 2012; 27(1): 14-26.

[13] Yao J, Li H, Liao Y, Chen Z. An improved control strategy of limiting the DC-link voltage fluctuation for a doubly fed induction wind generator. IEEE Trans. on Power Electronics 2008; 23(3): 1205-1213.

[14] Passino K. M, Yurkovich Y. Fuzzy Control, Addison-Wesley, Longman, Menlo Park, CA, 1997, p. 10.

[15] Zeng G. Q, Hu J. A, Wang D, Liu C. L. Fuzzy control theory and engineering application. Huazhong University of Science and Technology Press, Wuhan, China, 2006, pp. 86.

[16] Takagi T, Sugeno M. Fuzzy identification of systems and its application to modeling and control. IEEE Transactions on Systems, Man and Cybernetics 1985; 15(1): 116-132.

[17] Dianguro X, Na H, Wei W. Study on fuzzy controller with a self-adjustable factor of active power filter. Annual Conference of the IEEE Industrial Electronics Society, Paris, France, November 2006.

[18] Chen Z, Gomez S. A, McCormick M. A fuzzy logic controlled power electronic system for variable speed wind energy conversion systems. Eighth International Conference on Power Electronics and Variable Speed Drives, London, UK, 2000, pp. 114-119.

[19] Akbiyik B, Eksin I, Guzelkaya M. Evaluation of the performance of various fuzzy PID controller structures on benchmark systems. 4th International Conf. on Electrical and Electronics Engineering, Bursa, Turkey, 2005, pp. 388-393.

[20] Xia H, Song J. C. Development of fuzzy PID controller. Survey of Chemical Industry 2003; 11(7): 1-5.

[21] Reznik L, Ghanayem O, Bourmistrov A. PID plus fuzzy controller structures as a design base for industrial application. Engineering Application of Artificial Intelligence, 2000, pp. 419-430.

[22] Cheng M, Sun Q, Zhou E. New self-tuning fuzzy PI control of a novel doubly salient permanent-magnet motor drive. IEEE Transactions on Industrial Electronics, June, 2006; 53(3): 814-821.

[23] Li W. Design of hybrid fuzzy logic proportional plus conventional integral-derivative controller. IEEE Trans. Fuzzy Systems 1998; 6(4): 449-463.

[24] Kim Y. T, Bien, Z. Robust self-learning fuzzy controller design for a class of nonlinear MIMO system. Fuzzy Sets and Systems 2000; 111, 117-135.

[25] Aissaoui A. G, Tahour A, Essenbouli N, Nollet F, Abid M. & Chergui M. I. A Fuzzy-PI control to extract an optimal power from wind turbine. Global Conference on Renewables and Energy Efficiency for Desert Regions and Exhibition, GCREEDER 2011, Amman-Jordan, 26-28 April 2011.

[26] Labiod S, Boucherit M. S. Direct stable fuzzy adaptive control of a class of SISO nonlinear systems. Arch. Control Sci. 13(1): 95-110.

IntechOpen